第 XX 卷第 XX 期
XXXX 年XX 月
土 木 与 环 境 工 程 学 报(中 英 文)
Journal of Civil and Environmental Engineering
Vol. XX No. XX
XX XXXX

DOI: 10.11835/j.issn.2096-6717.2025.114
开放科学(资源服务)标识码OSID:

变化渗流场作用下边坡动态稳定性分析与可靠性评价

雷德明[1],仉文岗[2],何祥嵘[2],吴嘉昊[2],王林[3],张仁利[4],涂春华[5],王鲁琦[2],邹育麟[1]

(1. 四川沿江攀宁高速公路有限公司,四川 西昌 615000; 2. 重庆大学 土木工程学院,重庆 400045; 3. 北京师范大学 国家安全与应急管理学院,广东 珠海 519087; 4. 重庆高速公路集团有限公司,重庆 401121; 5. 重庆顶级信息有限公司,重庆 401120)

摘　要: 坝坡失稳将直接影响大坝工程的防洪、发电等关键功能,降雨、水位波动、地震作用以及边坡岩土参数的固有不确定性是导致坝坡失稳的主要因素。目前针对上游与下游坝坡稳定性的对比研究仍较匮乏,尤其是在系统考虑空间变异性的情况下。以某大坝为工程背景,基于实际地形、水文及地震资料构建渗流-稳定性数值模型,结合当地水位变化、降雨及历史地震记录开展为期一年的单因素确定性分析,并进一步将黏聚力与内摩擦角建模为随机场,在多因素共同作用下开展坝坡失效概率评估及敏感性分析。结果表明,上游坝坡在水位下降速率较高的情况下敏感性更强,失效概率显著升高。随机场分析显示空间变异性会显著影响失效概率的分布特征,说明其在可靠性评估中不可忽视。同时,黏聚力变异系数、水平地震系数越大以及黏聚力与内摩擦角相关性越强,坝坡稳定性越差。

关键词: 上游坝坡;下游坝坡;多诱发因素;稳定性分析;可靠性评估

中图分类号: TV641　　**文献标志码:** A　　**文章编号:** 2096-6717(XXXX)XX-0001-13

Dynamic stability analysis and reliability assessment of slopes under varying seepage fields

LEI Deming[1], ZHANG Wengang[2], HE Xiangrong[2], WU Jiahao[2], WANG Lin[3], ZHANG Renli[4], TU Chunhua[5], WANG Luqi[2], ZOU Yulin[1]

(1. Sichuan Yanjiang Panning Expressway Co., Ltd., Xichang 615000, Sichuan, P. R. China; 2. School of Civil Engineering, Chongqing University, Chongqing 400045, P. R. China; 3. School of National Safety and Emergency Management, Beijing Normal University, Zhuhai 519087, Guangdong, P. R. China; 4. Chongqing Expressway Group Co., Ltd., Chongqing 401121, P. R. China; 5. Chongqing Top Information Co., Ltd, Chongqing 401120, P. R. China)

Abstract: Slope instability may impair the key functions of a dam, such as flood control and power generation. Rainfall, water level fluctuation, seismic action, and the inherent uncertainty of geotechnical parameters are major factors that can trigger dam-slope failure. However, comparative studies focusing on the stability of upstream and downstream slopes remain limited, particularly when spatial variability is systematically

Received: 2025-09-01

Foundation items: Special Funding for Postdoctoral Scientific Research Projects in Sichuan Province (TB2024023); Sichuan Transportation Science and Technology Project (2018-ZL-01)

Author brief: LEI Deming (1979-), senior engineer, main research interest: highway construction management, E-mail: 420675702@qq.com.

HE Xiangrong (corresponding author), PhD candidate, E-mail: hexiangrong662021@163.com.

considered. In this study, a seepage-stability coupled numerical model is established using the actual topography, hydrological conditions, and seismic records of a selected dam. Based on local water level variation, rainfall, and historical earthquake data, one-year deterministic analyses under single factor conditions are performed. Cohesion and friction angle are then modeled as random fields, and the slope failure probability under the combined effects of multiple triggering factors is evaluated, followed by parameter sensitivity analysis. The results indicate that the upstream slope exhibits higher sensitivity under rapid water level drawdown conditions, leading to a marked increase in failure probability. The random field analysis highlights that spatial variability significantly affects the distribution of failure probability, underscoring its importance in reliability assessment. Furthermore, larger coefficients of variation of cohesion, higher horizontal seismic coefficients, and stronger correlation between cohesion and friction angle all contribute to reduced slope stability.

Keywords: upstream slope; downstream slope; multiple triggering factors; stability analysis; reliability evaluation

1 Introduction

The stability of dam slopes has always been a significant area of concern to hydropower engineers. Managing slope stability not only benefits construction but also greatly helps in reducing maintenance cost[1-3]. In recent years, major landslides, exemplified by the Hushan landslide at the Longyangxia hydropower station, the Baige landslide along the Jinsha River, and the Jinpingzi giant landslide at the Wudongde hydropower station, have not only caused substantial loss of life and property but have also attracted widespread attention from scholars[4-7]. Investigating the failure mechanisms of dam slopes under multiple triggering factors is thus of significant importance and urgency as it offers valuable recommendations and guidance for the construction and maintenance of similar projects.

The single or combined effects of rainfall, water level fluctuation, and earthquakes are widely considered to be the primary causes of dam slope instability[8-10]. Koyama et al. [11] attributed recent landslides in Japan primarily to intense rainfall and dam water level fluctuations, and Chen et al. [7] conducted a study on the instability mechanism of the Baige landslide under the combined effects of rainfall and earthquakes and identified the cause of the formation of a dammed lake along the Jinsha River. Numerous scholars have also conducted sensitivity analysis on slopes under water level fluctuations and found that slope gradient and water head height are the main controlling factors for slope stability, with the most significant impact occurring during rapid water level drops[12-14]. However, there is relatively limited research on the stability of dams under the combined effects of the three factors and considering the spatial variability[15-16] even though this is a practical issue that must be analyzed and studied due to its significant importance for early construction warnings and guidance. Additionally, there has been limited research on the comparative study of the stability between the upstream and downstream slopes of a dam. Existing studies primarily emphasize the analysis of downstream slopes in the traditional sense but neglect the stability and trend variations in the slopes on the other side of the dam[11, 17-19].

In this paper we modeled a specific dam was using finite element numerical simulation of a two-dimensional seepage field, slope limit equilibrium methods (LEM), and the Newmark displacement method. This analysis of the dam body was conducted based on ten years of rainfall data, measured dam water level fluctuations, and historical seismic data in the dam study area. The spatial variability of dam parameters was characterized using the random field method, and the failure probability of the dam slope was calculated using Monte Carlo simulation. The influence of random statistical variables including the coefficient of variation (COV), correlation coefficient, and scale of fluctuation on the failure probability of the dam slope is then discussed (a flow chart of deterministic and probabilistic analysis of the specific dam is shown in Fig. 1).

2 Study area

2.1 Geographic location

The dam study area in this paper has an overall topography that is higher in the south and lower in

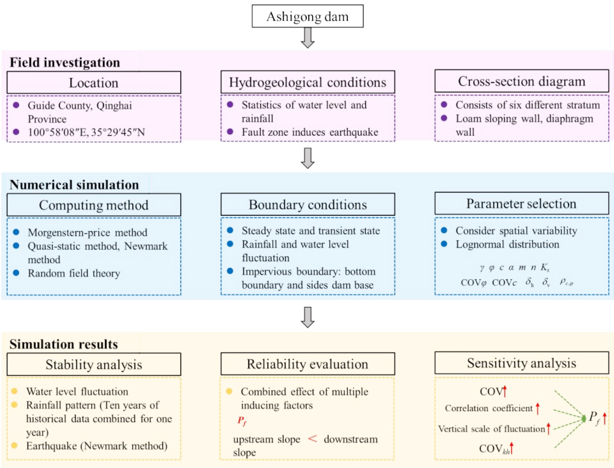

Fig. 1　Flow chart of deterministic and probabilistic analysis of the dam

the north, with elevations ranging between 2 170 m and 4 399 m. Its central area is relatively depressed, creating a basin encircled by mountains on all sides. The terrain is characterized by contiguous mountains and numerous valleys, comprising high mountains, middle mountains, low hills, and river valley plains. Geographically, the study area is bordered by Huangyuan and Huangzhong to the north, Gonghe and Guinan to the west, Zeku and Tongren to the south, and Jianzha and Hualong to the east. The S201 highway traverses the entirety of the dam's county.

The specific dam project is located in Hainan Tibetan Autonomous Prefecture, Qinghai Province (100°58′08″E-101°47′50″E, 35°29′45″N-36°23′35″N). Positioned between the Longyangxia and Lijiaxia sections of the upper Yellow River, the dam site is approximately 18.9 km upstream from the hydrological station. The Yellow River flows through this region from east to west, and it is situated about 25 km away from the center of the county town.

2.2　Hydrology and geological engineering conditions

The dam study area is situated in the deep inland region on the edge of the Qinghai-Tibet Plateau, which is characterized by a plateau continental climate with abundant sunlight and significant diurnal temperature variations. According to data from the hydrometeorological station in December, 2022, the annual average temperature is 7.2℃, and the annual average precipitation ranges from 251 to 459 mm. As shown in Fig. 2, the county exhibits distinct vertical zonation characteristics in terms of climate, with rainfall gradually increasing with elevation and slightly higher in the eastern part compared to the western part. From a temporal perspective, rainfall in the region exhibits significant seasonal variability as well. As illustrated in Fig. 3, precipitation over the past five years has predominantly occurred during summer and autumn, with July and August alone contributing to more than 45% of the yearly total. Historical records further show that the majority of maximum daily rainfall events are between 20.0 mm and 25.0 mm, which qualifies as heavy rainfall.

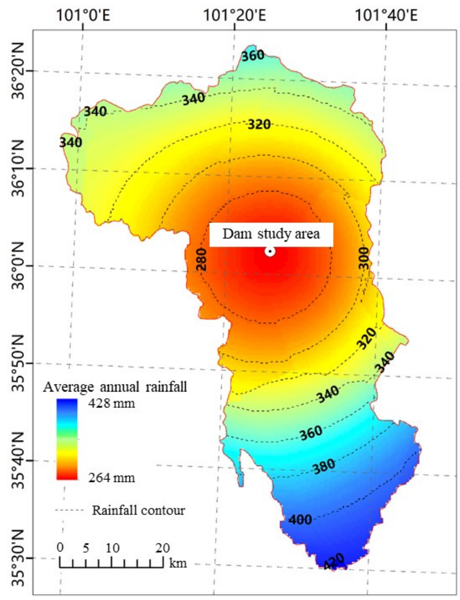

Fig. 2　Historical rainfall contour map of the study area

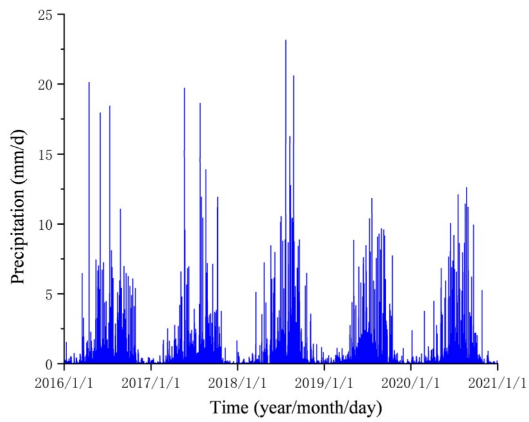

Fig. 3　Rainfall in the study area over the most recent five years

According to the stratigraphic division defined by Qinghai Province, the surveyed area consists of the Southern Qilian subregion of the Qilian Formation and the Hainan subregion of the Qinling Formation. The major exposed strata in these subregions include the Cambrian (Є), Permian of the Paleozoic Era (P), Neogene of the Cenozoic Era (N, E), and

Quaternary (Q), and the profile of the specific dam is illustrated in Fig. 4. A deep and large fault zone serves as the primary cause of seismic activity in this specific area, and the seismic intensity in the dam's area is generally categorized as VII. The peak ground acceleration of the seismic motion has been recorded as 0. 10g.

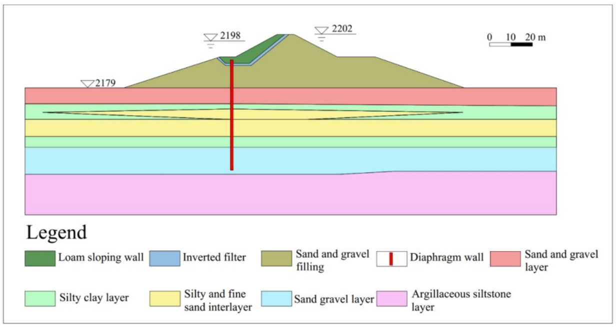

Fig. 4 The profile of the specific dam

3 Methodology

3. 1 Limit equilibrium method

The limit equilibrium method (LEM) is a widely used traditional technique for assessing slope stability by analyzing the force balance within a potential failure mass. This approach typically segments the slope into multiple vertical slices, with stability determined by evaluating the equilibrium of these individual segments. Variations in slice interaction assumptions give rise to different analytical methods.

Among these, the Morgenstern-Price method is recognized for its comprehensive nature, as it simultaneously satisfies both force and moment equilibria. It also introduces a customizable function to model the distribution of interslice shear forces, which enhances its capability to simulate complex slope behaviors more accurately.

3. 2 Pseudo-static method

The pseudo-static method is based on the limit equilibrium method for calculating the safety factor. It involves applying an equivalent horizontal or vertical static force to represent the seismic action at the center of gravity of each soil or rock section. Subsequently, conventional calculations are carried out based on these static equilibrium relationships, and the static force can be expressed as follows:

$$F_i = \frac{\alpha Q_i}{g} = kQ_i \tag{1}$$

where F_i denotes the inertial force acting on the i-th soil or rock segment; α represents the pseudo-static acceleration; Q_i stands for the weight of the i-th segment; and k is the seismic coefficient. The pseudo-static method determines the slope stability by comparing and calculating the minimum safety factor. However, it neglects the fact that earthquakes are transient but highly complex processes. Solely considering the minimum values often leads to overly conservative evaluations. Therefore, many scholars have made improvements to the pseudo-static method, such as considering the average safety factor and treating seismic coefficients as random variables[20].

3. 3 Newmark sliding block method

When the peak ground acceleration of an earthquake exceeds the yield acceleration, the sliding body begins to slide. By integrating the actual acceleration that causes the sliding of the body, the permanent displacement under the condition of instability during the earthquake action can be obtained. By comparing this displacement with a predetermined allowable value, the safety of the dam body can be evaluated. Newmark obtained a regression model for permanent displacement and yield acceleration through experiments, expressed as follows[21]:

$$u = \frac{v_{\max}^2}{2a_y}\left(1 - \frac{a_y}{A}\right) \tag{2}$$

where u represents permanent displacement; v_{max} denotes peak ground velocity; a_y is yield acceleration; and A represents peak ground acceleration. Furthermore, based on actual historical earthquake acceleration time-history curves, Newmark also provided a calculation formula for the conservative maximum displacement of the sliding mass:

$$u_{\max} = \frac{v_{\max}^2}{2a_y}\left(\frac{A}{a_y}\right) \tag{3}$$

4 Parameter selection and model establishment

4. 1 Numerical model and boundary conditions

Considering the actual engineering conditions and typical geological characteristics of the dam in question, a two-dimensional seepage model incorporating both saturated and unsaturated zones was constructed using SLIDE2 (Fig. 5). The dam itself has a base width of 147 m and a height of 23 m, and its foundation extends 225 m in width and 50 m in depth. Its stratigraphic sequence from surface to base comprises sand and gravel fill, a sand and gravel layer, silty clay, an interlayer of silty and fine sand, an additional sand gravel layer, and finally, an argillaceous siltstone layer. The model operates under two types of boundary conditions: steady-state and transient. To control variables effectively, a fixed water level of 2 m is applied to the right side of the dam, meaning that water level variations occur only on the left side where they from 9 m to 19 m. Rainfall infiltration is modeled above the intersection between the dam crest and the water surface. In the steady-state analysis, both the initial condition and the water level on the right side are defined as constant head boundaries, and other regions are assigned variable head conditions. Moreover, the lateral boundaries of the dam foundation and the bottom of the argillaceous siltstone layer are treated as impermeable.

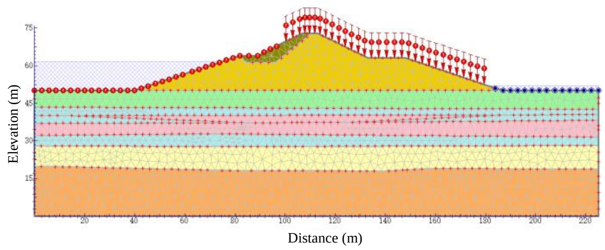

Fig. 5　Dam model and transient seepage boundary conditions

4.2　Determination of geotechnical parameters

In order to obtain accurate engineering mechanics parameters, we utilizing field survey data, hydrogeological information, and engineering geological parameters. Due to the nonuniform distribution of the dam body, it was necessary to consider the randomness of the geotechnical parameters[22, 23]. Hence, in the modeling and calculation processes of this study, the randomness of cohesion (c) and internal friction angle (φ) were both taken into account, and further investigation was carried out on employing the random field method to simulate the spatial variability of the geotechnical material. By setting parameters such as mean, variance, scale of fluctuations, and autocorrelation function, a more reasonable representation of the spatial variability of the geotechnical material was achieved. Furthermore, we referenced the geological survey reports and relevant papers by Li et al. [24] and Liu et al. [25] to estimate the physical and hydraulic parameters of the dam body and dam foundation, which are listed in Table 1 and Table 2. In addition, these parameters were cross-checked with laboratory test data on representative soil and rock samples collected from the study site. Field monitoring records, including groundwater levels and permeability test results, were also considered to ensure the reliability of parameter ranges. For strata without sufficient site-specific measurements, parameter values were inferred from comparable geological formations reported in the literature.

The provided parameters in these tables serve as baseline values for subsequent sensitivity analysis in the following sections. Both the dam body and dam foundation are assumed to follow lognormal distributions. Additionally, when considering random field variables, the fluctuation ranges of all parameters, except for the fluctuation range of dam body parameters ($\delta_v = 4$ m, $\delta_h = 40$ m), were set to $\delta_v = 2$ m and $\delta_h = 20$ m, and the baseline values for the correlation coefficient ($\rho_{c,\varphi}$) were all set to -0.5.

Table 1　Physical and mechanical parameters of the dam

Soil type	Unit weight γ/(kN/m^3)	Cohesion c/kPa	Friction angel φ/(°)	α	m	n	Permeability coefficient K_s/(m/s)
Dam body	22	85	29	5	2.68	0.39	5×10^{-5}
Sand and gravel layer	19.9	0	27	-	-	-	3.2×10^{-5}
Silty and fine sand interlayer	19.9	0	21	-	-	-	5×10^{-7}
Silty clay layer	18.8	16	11	-	-	-	5×10^{-6}
Sand gravel layer	21.2	0	30	-	-	-	3.2×10^{-5}

Modern stability analysis of dam slopes commonly relies on the limit equilibrium method or the strength reduction method to derive safety factors as evaluation criteria. However, for dam slopes that are subjected to seismic conditions, the Newmark sliding block displacement method is also utilized to assess slope stability[26]. In this study, a safety factor of 1.2 was chosen as the critical threshold for determining

Table 2 Probabilistic geotechnical parameters of dam materials

Soil type	Parameters	Mean	COV	Distribution	Scale of fluctuation	Correlation coefficient
Dam body	c	85	0.5	Lognormal	$\delta_h=40m$, $\delta_v=4m$	$\rho_{c,\varphi}=-0.5$
	φ	29	0.2			
Sand and gravel layer	c	0	-	Lognormal	$\delta_h=20m$, $\delta_v=2m$	$\rho_{c,\varphi}=-0.5$
	φ	27	0.2			
Silty and fine sand interlayer	c	0	-	Lognormal	$\delta_h=20m$, $\delta_v=2m$	$\rho_{c,\varphi}=-0.5$
	φ	21	0.2			
Silty clay layer	c	16	0.5	Lognormal	$\delta_h=20m$, $\delta_v=2m$	$\rho_{c,\varphi}=-0.5$
	φ	11	0.2			
Sand gravel layer	c	0	-	Lognormal	$\delta_h=20m$, $\delta_v=2m$	$\rho_{c,\varphi}=-0.5$
	φ	30	0.2			

the stability of dam slopes after accounting for engineering practicality and the potential consequences of slope failures.

5 Results

5.1 Stability analysis under a change in a single factor

A deterministic evaluation of the dam was conducted based on historical rainfall records from the study region, observed upstream hydropower station water levels, and representative seismic acceleration time-history curves captured in Changu Town during the Yushu earthquake in Qinghai. This assessment covered a one-year period and involved step-by-step design and analysis under three separate scenarios: water level fluctuation, precipitation distribution, and seismic loading.

5.1.1 Water level fluctuation

To evaluate the influence of water level fluctuation on dam slope stability, recent one-year observational data from the Lijiaxia Hydropower Station were employed. The entire analysis was segmented into four distinct phases, as shown in Fig. 6 - Fig. 9.

Stage Ⅰ (March 1 - May 31): In this stage, the stability of both upstream and downstream slopes generally improves. The lowest water level is observed on April 15. A notable delayed response is observed on the downstream slope, where the safety factor continues to increase even after the water level reaches its minimum. Conversely, the upstream slope exhibits a more immediate response, likely due to its direct connection with the reservoir, allowing the phreatic surface to adapt more swiftly to fluctuations in water level.

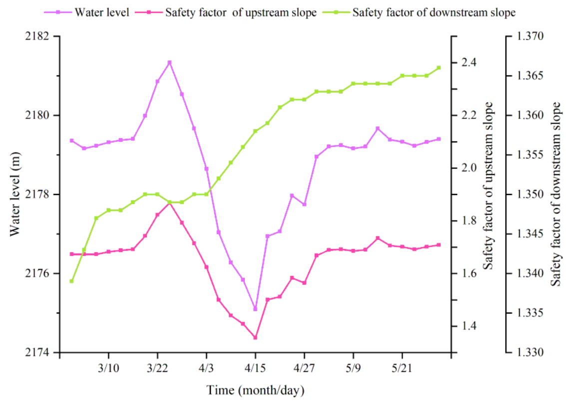

Fig. 6 Stability variation in upstream and downstream slopes during Stage Ⅰ

Stage Ⅱ (June 1 - August 31): An inverse relationship in stability is observed between the upstream and downstream slopes. The safety factor of the upstream slope strongly correlates with water level variations, and the downstream slope follows an opposite pattern. By the end of this stage, the upstream slope's safety factor stabilizes around 1.75, whereas the downstream slope levels off near 1.368, indicating superior stability on the upstream side.

Stage Ⅲ (September 1 - November 30): During

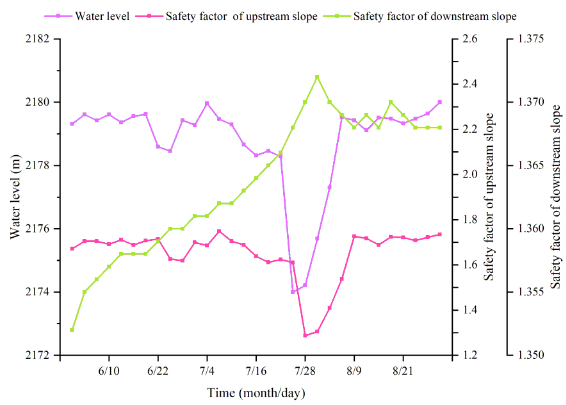

Fig. 7 Stability variation in upstream and downstream slopes during Stage Ⅱ

this period, the safety factor of the upstream slope closely tracks fluctuations in water level. A sharp decrease in water level causes a significant reduction in the upstream slope's stability. In contrast, the downstream slope's safety factor continues to rise, again showing a delayed reaction. The maximum safety factor variation for the upstream slope is 19.96%, notably higher than the 1.60% observed for the downstream slope. This disparity indicates the greater sensitivity of slopes adjacent to the water body to water level changes. Stage Ⅱ; (c) Stage Ⅲ; (d) Stage Ⅳ

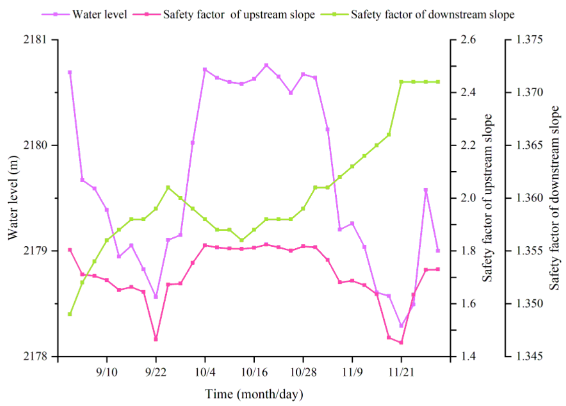

Fig. 8　Stability variation in upstream and downstream slopes during Stage III

Stage Ⅳ (December 1 - February 28): The trend during this final stage is comparable to the previous one. The upstream slope continues to exhibit a response aligned with water level changes, and the downstream slope shows a moderate and delayed increase in its safety factor.

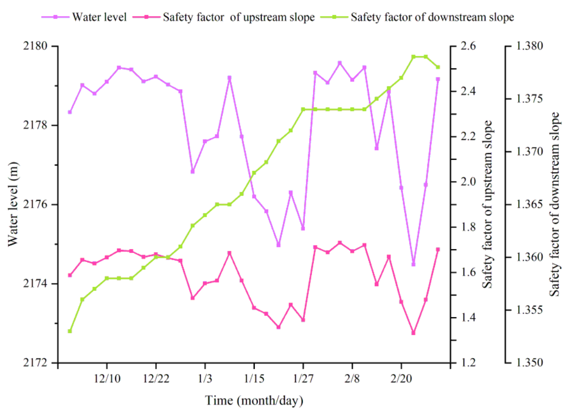

Fig. 9　Stability variation in upstream and downstream slopes during Stage IV

5.1.2　Rainfall

The region where the dam is located experiences relatively low levels of rainfall. Therefore to understand the impact of rainfall on stability, historical rainfall data from the past 10 years (2010-2020) in the area were compiled, and the highest daily rainfall value for each year was extracted to synthesize the annual rainfall. As illustrated in Fig. 10, the actual rainfall in the area has a minimal effect on the stability of the dam slopes. Consistent with the previous analysis, the stability of the upstream slope is greater than that of the downstream slope. Quantitatively, the maximum variations in the safety factor for the upstream and downstream slopes throughout the year are 0.099% and 0.074%, respectively. Furthermore, over the entire calculation period, the safety factor of the downstream slope undergoes only two changes, one less than the changes observed in the upstream slope, indicating that the upstream slope is more sensitive to rainfall.

5.1.3　Earthquakes

To evaluate the stability of the upstream and downstream slopes under practical operating conditions more precisely, we used the Newmark sliding block method for displacement analysis. The seismic record from Changu Town, Qinghai Province, was input into SLIDE2, and the corresponding results are illustrated in Fig. 11 and Fig. 12. The analysis under seismic loading consistently revealed that the downstream slope possesses lower stability than the upstream slope. Additionally, the installation of anti-slide piles on the left side results in a comparatively larger slip surface on the upstream slope than on the downstream side.

5.2　Reliability evaluation under the combined action of multiple factors

Fig. 13 illustrates the safety factor variations for both the upstream and downstream slopes throughout the annual calculation period. The upstream slope's safety factor fluctuates between 1.288 and 1.854 and follows a trend similar to water level changes. In contrast, the downstream slope's safety factor remains within a narrower range of 1.351 to 1.382 and shows a gradual upward trend. A clear lag effect in the downstream slope's safety factor is evident at the end of February and early June, which aligns with the findings discussed in the previous section.

Fig. 14 illustrates the variation in failure probability for both the upstream and downstream dam

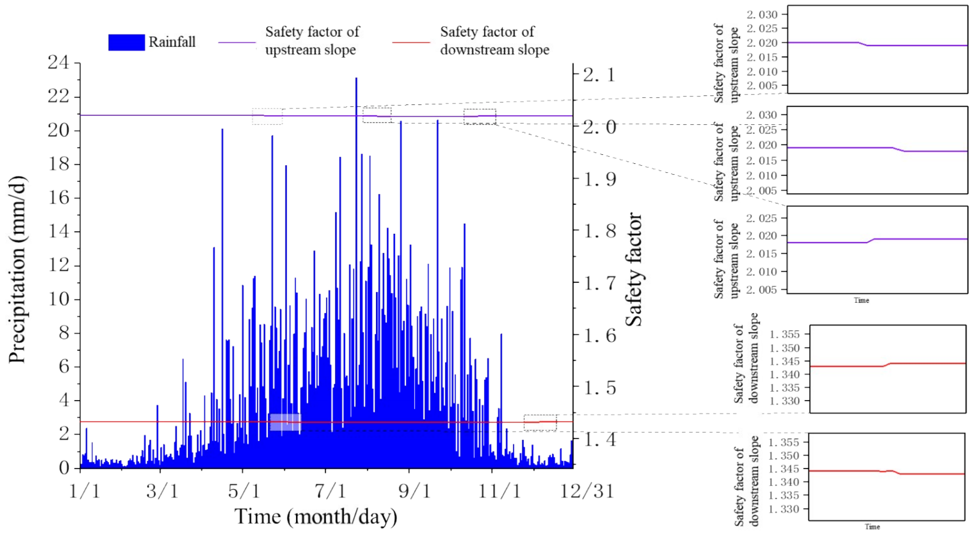

Fig. 10 Stability variation in the dam slope due to rainfall

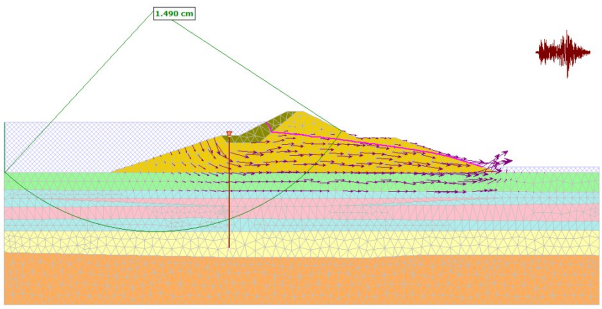

Fig. 11 Stability of the upstream slope calculated using the Newmark method

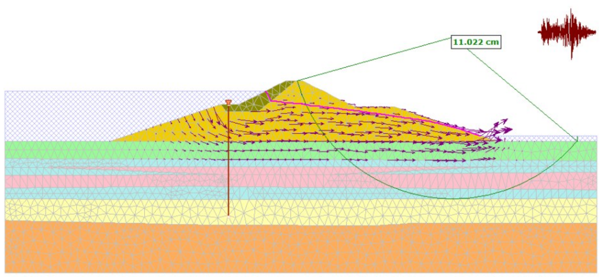

Fig. 12 Stability of the downstream slope calculated using the Newmark method

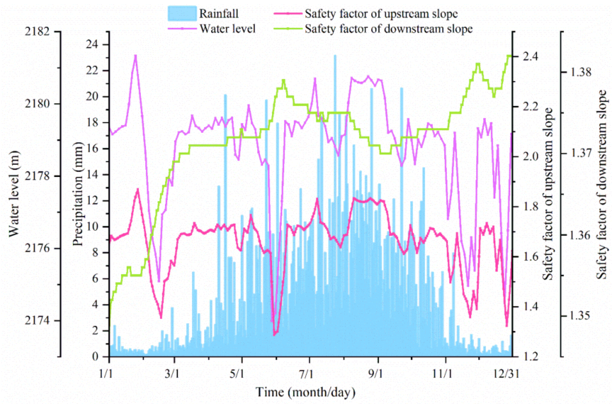

Fig. 13 Annual variation in the dam's safety factor

slopes over the course of the entire annual calculation period. The failure probability of the upstream slope remains largely at zero, with notable peaks occurring during four extreme low water level events. The most critical instance is in June, when the failure probability of the upstream slope reaches 15.03%. In contrast, the failure probability of the downstream slope typically stays below 1.5%, with its highest value occurring early in the calculation period and gradually declining to a minimum of 0.15% by the end of the year. It is thus evident that significant fluctuations in the failure probabilities of both slopes coincide with substantial water level changes, highlighting the more pronounced effect of water level fluctuations on the dam's failure probability compared to rainfall. Although the failure probability of the upstream slope remains nearly zero throughout the year and that of the downstream slope stays above zero, it is the upstream slope that poses a higher risk of dam instability even though the downstream slope may initially seem more vulnerable.

5.3 Sensitivity analysis

The difference in failure probability of the upstream slope of the dam is more pronounced between the 150^{th} and 154^{th} days, and this time interval spans five consecutive days. Therefore, this time period was chosen for conducting the sensitivity analysis of spatial variability parameters for the upstream slope of the dam.

5.3.1 Comparison between the random field model

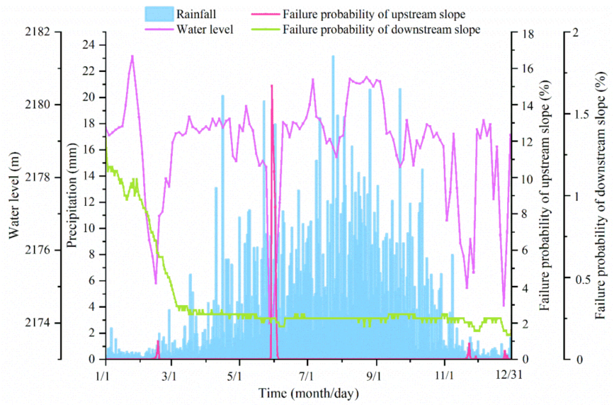

Fig. 14　Annual variation in dam failure probability

and the random variable model

The cohesion (c) and internal friction angle (φ) of the dam are often considered as the two primary random variables for calculating slope reliability. However, since soil and rock materials are widely distributed and possess spatial variability, this variability should be taken into account[27, 28]. Parameters for both the random field and random variable models are selected according to Table 2. Analysis of Fig. 15 reveals that within a five-day calculation period, the failure probability of the upstream slope decreased by 12.79% in the random field model and by 1.12% in the random variable model, compared to the initial baseline condition. This significant difference between the two models highlights the fact that depending solely on the random variable model in traditional calculations could lead to an underestimation of the dam slope's failure probability, thus elevating risks in slope engineering. However, some researchers have pointed out that, in certain specific slope models, accounting for the spatial variability of soil and rock materials may also result in a lower estimation of the slope failure probability[29].

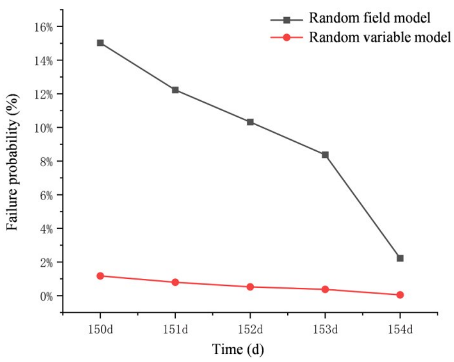

Fig. 15　Comparison between the random field and random variable models

5.3.2　The effect of the COV

In the field of geotechnical engineering, data indicate that the coefficient of variation of the internal friction angle (COV_{φ}) is generally smaller than the coefficient of variation of the cohesion (COV_c)[30]. Consequently, COV_{φ} values were varied within the range of 0.1, 0.15, 0.2, 0.25, and 0.3, and COV_c values were varied within the range of 0.1, 0.2, 0.3, 0.4, and 0.5. When assessing the impact of COV_{φ} variations on the failure probability, COV_c was kept as the baseline, and vice versa.

As shown in Fig. 16 and Fig. 17, the failure probability shows minimal change when COV_{φ} varies within the specified range. For example, on the 150th day, a change in COV_{φ} from 0.1 to 0.3 results in a slight increase in failure probability from 15.01% to 16.02%. In contrast, variations in COV_c have a more significant effect on failure probability. On the same day, when COV_c increases from 0.1 to 0.5, the failure probability rises from 9.03% to 15.02%. Both COV_{φ} and COV_c negatively impact slope stability, with cohesion having a more pronounced effect.

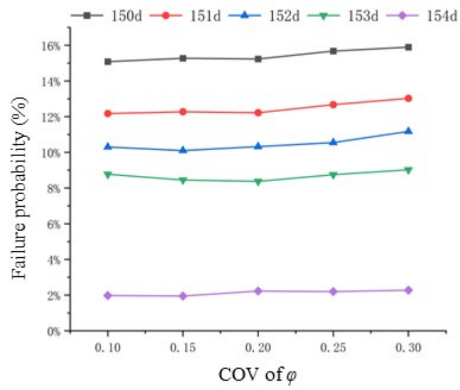

Fig. 16　Influence of COV_{φ} on failure probability

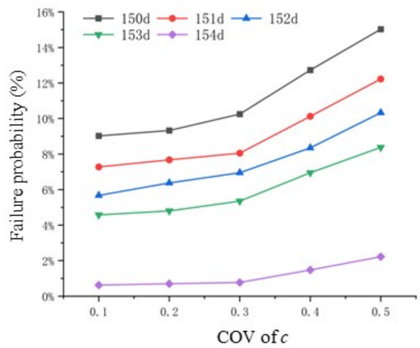

Fig. 17　Influence of COV_c on failure probability

5.3.3 The effect of the correlation coefficient

The cohesion (c) and internal friction angle (φ) of the dam body are not independent random variables; they typically exhibit a negative correlation, which can be quantified using their correlation coefficient ($\rho_{c,\varphi}$). In this study, the values of $\rho_{c,\varphi}$ were taken to be -0.5, -0.3, 0, 0.3, and 0.5. As illustrated in Fig. 18, a decrease in the correlation coefficient, indicating a stronger negative correlation, results in a reduced slope failure probability. For instance, on the 150th day, when $\rho_{c,\varphi}$ = -0.5, the failure probability is 15.02%, whereas it rises to 21.73% when $\rho_{c,\varphi}$ = 0.5. Furthermore, the impact of the correlation coefficient on failure probability decreases over time, likely because the probability reaches a smaller value, limiting spatial variation.

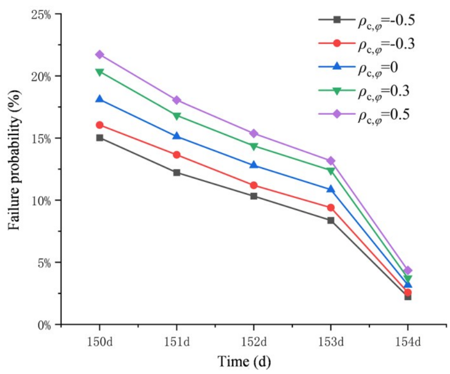

Fig. 18 The influence of correlation coefficient on failure probability

5.3.4 The effect of the scale of fluctuation

The scale of fluctuation refers to the maximum distance over which parameters of rock and soil remain correlated in a spatially variable random field. It is divided into the vertical scale of fluctuation (δ_v) and the horizontal scale of fluctuation (δ_h). In practice, the horizontal correlation of rock and soil is significantly larger than the vertical correlation. Therefore, in this study, the vertical scale (δ_v) was varied at 2 m, 4 m, 6 m, 8 m, and 10 m, and the horizontal scale (δ_h) was adjusted at 20 m, 40 m, 60 m, 80 m, and 100 m.

In Fig. 19 and Fig. 20, it is clear that although the vertical scale is smaller than the horizontal scale, it exerts a more pronounced influence on failure probability. For example, on the 150th day, increasing δ_v from 2 m to 10 m raises the failure probability from 14% to 18.4%, and changing δ_h from 20 m to 100 m decreases the failure probability from 16.48% to 13.95%. Overall, the effects of the vertical and horizontal scales of fluctuation on the dam's failure probability show opposite trends. Specifically, the failure probability increases with δ_v but decreases with δ_h. This phenomenon can be explained by the fact that vertical heterogeneity directly governs the distribution of seepage pathways and the mobilization of shear strength along potential slip surfaces. A larger vertical correlation length implies more persistent weak zones extending through the depth of the slope, which can significantly reduce stability. In contrast, a larger horizontal correlation length tends to average out local weaknesses over a broader spatial extent, thereby reducing their adverse influence on the overall failure probability.

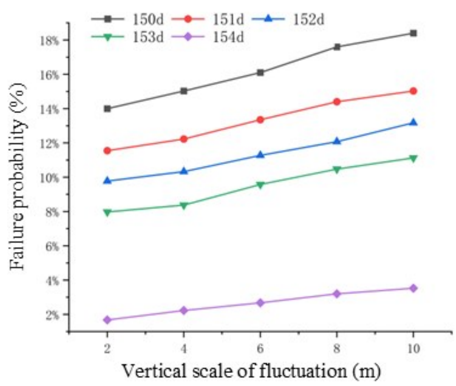

Fig. 19 The influence of vertical scale of fluctuation on failure probability

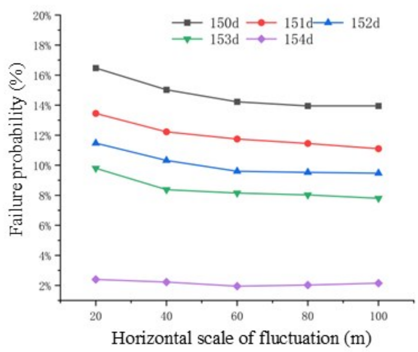

Fig. 20 The influence of horizontal scale of fluctuation on failure probability

5.3.5 The effect of the horizontal seismic coefficient

In this section, we investigate the influence of the coefficient of variation of the horizontal seismic coefficient (COV_{kh}) on the failure probability. The horizontal seismic coefficient (K_h) was set to a fixed value of 0.05, and COV_{kh} was varied at values of 0.1, 0.2, 0.3, 0.4, and 0.5. In Fig. 21, we see that the increase in failure probability is nonlinear as COV_{kh} increases; it is COV_{kh} on failure probability is more pronounced when COV_{kh} is smaller. As COV_{kh} exceeds 0.3, the increase in failure probability becomes less noticeable. Moreover, a lower COV_{kh} leads to a more significant reduction in failure probability over time. Overall, the coefficient of variation of the horizontal seismic coefficient plays a crucial role in determining the probability of failure of the dam.

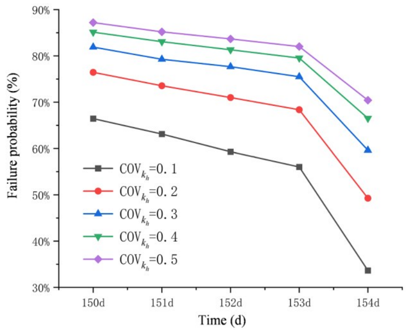

Fig. 21　The influence of COV_{kh} on failure probability

6　Discussion

6.1　Advantages of the proposed method

This study integrates spatial variability, water level fluctuation, rainfall, and seismic loading into a unified probabilistic framework. Compared to conventional deterministic or random-variable approaches, the method captures local heterogeneity more realistically and avoids underestimating failure probability.

6.2　Applicability and engineering relevance

The framework is particularly suitable for dam slopes that are subjected to multiple triggering factors. Our findings highlight the importance of monitoring upstream slopes during rapid drawdown events and support the use of early-warning thresholds and risk management strategies in hydropower projects.

6.3　Limitations and future directions

The present work employs a two-dimensional model and simplified rainfall conditions, which may not fully reflect complex three-dimensional failure mechanisms or long-term infiltration effects. Future research should therefore extend the framework to 3D modeling and incorporate diverse hydrological scenarios to enhance its generalizability.

7　Conclusions

Based on actual hydrological and engineering geological data, stability analysis and reliability evaluation were conducted on both the upstream and downstream slopes of a specific dam. Initially, a two-dimensional engineering geological model of the dam slopes was established using measured data. Subsequently, deterministic analysis was carried out separately for the upstream and downstream slopes under single-factor conditions, utilizing historical one-year period water level fluctuations, adjusted rainfall data, and seismic intensity data for the region. Furthermore, complete one-year period deterministic and probabilistic analyses were performed for these working conditions. Finally, sensitivity analysis of the statistical parameters of the random field model was conducted, resulting in the following main conclusions.

(1) The impact of actual rainfall in the region on dam stability is minimal, but earthquakes are the most significant external trigger for slope instability. Even under high-intensity seismic conditions, as determined by the Newmark sliding block displacement method, the slopes remain stable. The stability of the upstream slope shows a strong correlation with water level fluctuations, whereas the downstream slope exhibits a more noticeable lag effect and smaller stability variations compared to the upstream slope.

(2) By analyzing the safety factor variations of the upstream and downstream slopes under combined influencing factors over the course of a year, we found that the stability of the downstream slope generally improves, though the magnitude of this improvement is minor. Conversely, the stability of the upstream slope is largely influenced by water level changes, with safety factor variations closely following water level fluctuations and showing greater sensitivity to these changes than to rainfall. A one-year reliability evaluation revealed that although the failure probability of the upstream slope remains close to zero, the downstream slope consistently has a failure probability greater than zero. However, the upstream slope poses a greater risk under critical conditions.

(3) Incorporating spatial variability through a random field affects the assessment of dam slope reliability. Relying solely on a random variable model may lead to an underestimation of failure probability. Sensitivity analysis of dam body parameters for the upstream slope over a continuous 5-day period indicated that higher coefficients of variation for cohesion and horizontal seismic coefficient, a more positive correlation between cohesion and internal friction angle, and larger vertical fluctuations contribute to higher failure probability and reduced stability. Therefore, these parameters should be treated with particular caution in practical engineering applications.

(4) The current study is limited to a two-dimensional numerical framework and simplified rainfall conditions. Future work could extend the probabilistic framework to three-dimensional slope models in order to capture more complex spatial heterogeneity. In addition, incorporating variable rainfall boundary conditions, long-term infiltration effects, and coupled hydro-mechanical processes may further improve the generalizability and practical relevance of our proposed method.

References

[1] ZEWDU A. Modeling the slope of embankment dam during static and dynamic stability analysis: A case study of Koga dam, Ethiopia [J]. Modeling Earth Systems and Environment, 2020, 6(4): 1963-1979.

[2] CHARLES J A, BROMHEAD E N. Contributions to *Géotechnique* 1948 - 2008: Slope stability and embankment dams [J]. Géotechnique, 2008, 58(5): 385-389.

[3] ZHANG W G, HE X R, XU Q, et al. Investigation on internal evolution process of slope under seismic loading: Insights from a transparent soil test and shaking table test [J]. Transportation Geotechnics, 2024, 49: 101399.

[4] YUAN G X, WANG H, HUANG Z Q, et al. Study on the hysteresis effect of the stability of Longyangxia Dam Bank Slope with the fluctuation of water level [J]. Geofluids, 2023, 2023(1): 2476246.

[5] HUANG J X, DU W C, XIE M W. Numerical modeling of kinetic features and stability analysis of Jinpingzi landslide [J]. Land, 2023, 12(3): 679.

[6] ZHANG W G, MENG F S, CHEN F Y, et al. Effects of spatial variability of weak layer and seismic randomness on rock slope stability and reliability analysis [J]. Soil Dynamics and Earthquake Engineering, 2021, 146: 106735.

[7] CHEN Z, ZHOU H F, YE F, et al. The characteristics, induced factors, and formation mechanism of the 2018 Baige landslide in Jinsha River, Southwest China [J]. Catena, 2021, 203: 105337.

[8] SU Z Y, CHEN G Y, MENG Y. Study on seepage characteristics and stability of core dam under the combined action of the variation of reservoir water level and rainfall [J]. Geotechnical and Geological Engineering, 2021, 39(1): 193-211.

[9] WANG L, WU C Z, TANG L B, et al. Efficient reliability analysis of earth dam slope stability using extreme gradient boosting method [J]. Acta Geotechnica, 2020, 15(11): 3135-3150.

[10] HIMANSHU N, BURMAN A. Seepage and stability analysis of Durgawati earthen dam: A case study [J]. Indian Geotechnical Journal, 2019, 49(1): 70-89.

[11] KOYAMA A, FUJIMOTO T, SUETSUGU D, et al. Analysis of embankment failure mechanism in reservoirs due to rainfall infiltration during heavy rainfall [J]. Geomatics, Natural Hazards and Risk, 2022, 13(1): 1849-1866.

[12] SALIM S G, NOORI K M G. Assessment of the upstream slope stability of darbandikhan rockfill dam during drawdown [J]. Aro-the Scientific Journal of Koya University, 2021, 9(1): 8-15.

[13] LIANG J X, SUI W H. Sensitivity analysis of anchored slopes under water level fluctuations: A case study of Cangjiang bridge-Yingpan slope in China [J]. Applied Sciences, 2021, 11(15): 7137.

[14] TANG H M, WASOWSKI J, JUANG C H. Geohazards in the three Gorges Reservoir Area, China-Lessons learned from decades of research [J]. Engineering Geology, 2019, 261: 105267.

[15] ZHU X B, WANG X L, LI X, et al. A new dam reliability analysis considering fluid structure interaction [J]. Rock Mechanics and Rock Engineering, 2018, 51(8): 2505-2516.

[16] MOUYEAUX A, CARVAJAL C, BRESSOLETTE P, et al. Probabilistic stability analysis of an earth dam by Stochastic Finite Element Method based on field data [J]. Computers and Geotechnics, 2018, 101: 34-47.

[17] SU Z Y, ZHANG K L, LIU C D. Dynamic risk assessment of slope stability of homogeneous earth-rock dam under action of multiple hazards [J]. Simulation, 2022, 98: 699-710.

[18] WANG L, WU C Z, GU X, et al. Probabilistic stability analysis of earth dam slope under transient seepage using multivariate adaptive regression splines [J]. Bulletin of Engineering Geology and the Environment, 2020, 79(6): 2763-2775.

[19] JIANG S H, LIU X, HUANG J S. Non-intrusive reli-

ability analysis of unsaturated embankment slopes accounting for spatial variabilities of soil hydraulic and shear strength parameters [J]. Engineering with Computers, 2022, 38(S1): 1108.

[20] ZHANG S L, YIN Y P, HU X W, et al. Geo-structures and deformation-failure characteristics of rockslide areas near the Baige landslide scar in the Jinsha River tectonic suture zone [J]. Landslides, 2021, 18(11): 3577-3597.

[21] NEWMARK N M. Effects of earthquakes on dams and embankments [J]. Geotechnique, 1965, 15(2): 139-160.

[22] GUO X F, DIAS D, PAN Q J. Probabilistic stability analysis of an embankment dam considering soil spatial variability [J]. Computers and Geotechnics, 2019, 113: 103093.

[23] SANCHEZ LIZARRAGA H, LAI C G. Effects of spatial variability of soil properties on the seismic response of an embankment dam [J]. Soil Dynamics and Earthquake Engineering, 2014, 64: 113-128.

[24] LI D Q, JIANG S H, CAO Z J, et al. A multiple response-surface method for slope reliability analysis considering spatial variability of soil properties [J]. Engineering Geology, 2015, 187: 60-72.

[25] LIU L L, CHENG Y M, JIANG S H, et al. Effects of spatial autocorrelation structure of permeability on seepage through an embankment on a soil foundation [J]. Computers and Geotechnics, 2017, 87: 62-75.

[26] MIRCEVSKA V, NASTEV M, NANEVSKA A. Seismic slope displacement of tailings dam: A comparative study between modified Newmark and Mohr-Coulomb models [J]. Journal of Earthquake Engineering, 2022, 26(15): 7878-7900.

[27] ZHANG W G, GU X, HAN L, et al. A short review of probabilistic slope stability analysis considering spatial variability of geomaterial parameters [J]. Innovative Infrastructure Solutions, 2022, 7(4): 249.

[28] GRIFFITHS D V, FENTON G A. Probabilistic slope stability analysis by finite elements [J]. Journal of Geotechnical and Geoenvironmental Engineering, 2004, 130(5): 507-518.

[29] CHEN F Y, ZHANG R H, WANG Y, et al. Probabilistic stability analyses of slope reinforced with piles in spatially variable soils [J]. International Journal of Approximate Reasoning, 2020, 122: 66-79.

[30] CHO S E. Probabilistic assessment of slope stability that considers the spatial variability of soil properties [J]. Journal of Geotechnical and Geoenvironmental Engineering, 2010, 136(7): 975-984.

(编辑 XXX)